Finite Elements in Analysis and Design 48 (2012) 1392–1399

Contents lists available at SciVerse ScienceDirect

Finite Elements in Analysis and Design

journal homepage: www.elsevier.com/locate/finel

Dynamic analysis of cable-driven parallel manipulators with time-varying cable lengths

Jingli Du *, Hong Bao, Chuanzhen Cui, Dongwu Yang

Key Laboratory of Electronic Equipment Structure Design of Ministry of Education, Xidian University, Xi'an, Shaanxi 710071, China

ARTICLE INFO

Article history:
Received 28 January 2011
Received in revised form
18 August 2011
Accepted 18 August 2011
Available online 15 September 2011

Keywords:
Cable-driven manipulator
Time-varying cable length
Cable dynamics
Finite difference
Vibration

ABSTRACT

In conventional researches, cables of cable-driven parallel manipulators are treated as simple linear elements that can only work in tension. This results in the fact that the effect of cable dynamics on the positioning precision of the end-effector is not adequately taken into account. To overcome this shortcoming, a dynamic model for cable-driven parallel manipulators with cables of slowly time-varying length is presented in this paper. The partial differential equation characterizing the dynamics of a cable with varying-length is deduced, and converted into ordinary differential equations through spatial discretization by finite difference approximation. Then, the dynamic model for cable-driven parallel manipulators is achieved considering the relationship between the motion of the end-effector and the cable end force, in which the degrees of freedom of cables and the end-effector are all involved. Two numerical examples are demonstrated to validate the dynamic model, and also show that it is necessary to take into consideration the cable dynamics for manipulators of long-span cables.

1. Introduction

As one of the candidates of the implementation to the next generation radio telescope with the collecting area of up to one square kilometer, several Five-hundred-meter Aperture Spherical Telescope (FAST) are planning to be built by Chinese scientists in the Karst landform in southwest China [1], as shown in Fig. 1. Technically, the FAST has a number of innovations. Firstly, the feeds are suspended by a cable-supporting system, where 6 flexible cables move the feeds contained in a cabin within its workspace. This can reduce the structural weight considerably, leading to a feed-supporting structure of 20–30 ton. Secondly, a Stewart platform serving as the fine tuning system is added to the cabin to guarantee the required positioning accuracy of the feeds [2]. Thirdly, an active reflector is employed, whose illuminated part can be altered to a parabolic shape so that common point feeds can be utilized, dramatically enlarging the frequency bandwidth [3].

The cable-supporting system is a cable-driven parallel manipulator (CDPM) where the cabin serves as the end-effector, which is moved with 6 long-span varying length cables of several hundred meters long, as shown in Fig. 2. CDPMs work in the way similar to the rigid-link parallel manipulators, and possess nearly all the merits of the conventional parallel manipulators. CDPMs have several advantages [4]: (1) the overall mass and inertia of the manipulator are reduced since the cables are lightweight links; (2) they are less expensive and easier to build, transport, and reconfigure; (3) long cables can be easily stored on reels, providing the manipulators the possibility of potentially large workspaces. For these reasons, CDPMs seem to be the unique way to implement the feed-supporting structures for so large radio telescopes. For example, a CDPM is also adopted in the feed-supporting structure of the Large Adaptive Reflector, the Canadian design of the next generation radio telescopes [5]. The characteristics of the FAST CDPM include: (1) ultra large workspace; (2) high positioning precision; (3) slow motion that could be treated as in the static state, theoretically; (4) vibration of the end-effector attenuates very slowly due to the low damping of cables when it occurs for some reasons.

Many efforts have been devoted to modeling and control of CDPMs. Gouttefarde and Gosselin addressed the wrench-closure workspace of a planar fully constrained CDPM, and found an algorithm to determine its cross-sections [4]. Oh and Agrawal derived the dynamics of a 6 DOF CDPM and then utilized a reference governor-based controller with input constraint to guarantee that the cables can work in tension [6]. However, in most of these researches, cables are assumed to be linear elements that can only work in tension and the dynamical characteristics of cables themselves, such as the elastic elongation, vibrations, are neglected. For CDPMs of relatively small workspace or of lightweight cables, this assumption works reasonably; but for long-span cables, it does not work well. Therefore, considering the over long length of the cables in the FAST, we need a more accurate

* Corresponding author.
E-mail address: jldu@mail.xidian.edu.cn (J. Du).

0168-874X/$ - see front matter © 2011 Elsevier B.V. All rights reserved.
doi:10.1016/j.finel.2011.08.012

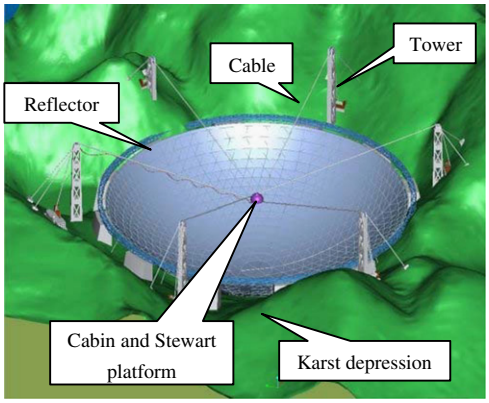

Fig. 1. Schematic of the FAST.

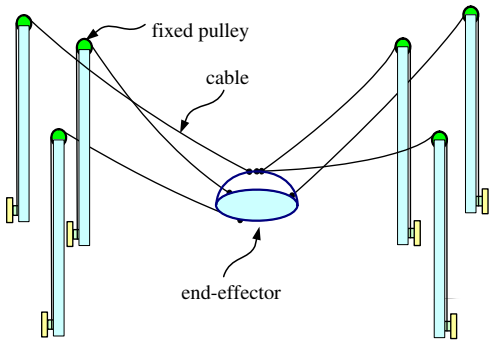

Fig. 2. Cable-supporting system of the FAST.

model to represent the cable dynamics in modeling the CDPM of the FAST.

A 50 m scaled model of the cable-supporting system is constructed to investigate the feasibility of the FAST concept. The mechanical analysis on the cable-supporting system has been carried out, such as the works in Refs. [7,8]. In these works it is pointed out that because of the long-span of cables and the slow motion of the manipulator, cable sags due to their gravity need to be considered but their dynamics can be omitted. However, during the operation of the cable-supporting system in the scaled model, vibrations of the cables, which result in vibration of the end-effector, can be observed. Many factors can cause these vibrations, such as initial position or velocity of the end-effector, operation of the fine-tuning Stewart platform, wind disturbance, speed reducer backlash, and friction of cables around fixed pulleys. To eliminate these vibrations efficiently dynamics of cables must be taken into consideration.

Koh and Rong performed the dynamic analysis of a three-dimensional cable, accounting for axial, flexural, torsional deformations and geometric non-linearity due to large displacements and rotations [9]. Chen and Ding investigated the transverse vibration of nonlinear strings, which is governed by partial differential equations, and developed a finite difference method to obtain the numerical solutions of these equations [10]. Gattulli et al. addressed the nonlinear dynamics and a longitudinal active control strategy for the suppression of cable oscillations [11]. However, in these works the effect of cable length variation was not taken into consideration. Terumichi et al. studied the nonstationary vibration of a string with time-varying length and a mass-spring system attached at the lower end, which was assumed to be the analytical model of an elevator [12]. Wang et al. investigated three dimensional underwater vibrations of a geometrically nonlinear cable with a time-dependent length [13]. Nevertheless, the initial stressed configuration of a cable was assumed to be a line and the cable was expected to undergo the axial motion in Refs. [12,13], therefore, applying these results to analyze the vibration of a cable moving freely in three dimensional space is a hard work. A dynamic model for the cable-supporting system was presented in Ref. [14], in which a partial-differential equation was utilized to describe the motion of cables. However, it did not give an efficient way to solve the equation when cable length varied.

This paper addresses modeling of the dynamics of CDPMs with the effects of the cable dynamics considered, which can be utilized to deal with the vibration of the manipulator. The governing equation for varying-length cables, which is a partial-differential equation, is first presented. The equation can be solved using the central difference algorithm for its spatial discretization when the cable length varies. Then, the dynamic model of CDPMs is deduced.

The organization of the paper is as follows: Section 2 presents the nonlinear dynamics equation of cables with time-varying length. And it is simplified for the case where cable length changes slowly and smoothly. Section 3 presents the finite-difference method to numerically solve the spatial discretization of the cable dynamic equation. The dynamic equation for CDPMs is achieved in Section 4 according to the relationship between the cable end force and the motion of the end-effector. Section 5 presents two examples to verify the effectiveness of the method. Some remarking conclusions are summarized in Section 6.

2. Dynamics of a varying-length cable

For each cable of the manipulator, one end is connected to the end-effector while the other end rolls though a pulley fixed at the top of its corresponding tower, and then is fed into a servo mechanism that controls the cable length. Consider a flexible cable of the unstretched length L with negligible bending and torsional stiffness. For a point P on the cable, the unstretched curve length along the average line of the cable is denoted by $s \in [0, L]$, and the corresponding stretched length by s_e. Thus the axial strain of the cable is

$$\varepsilon = \frac{ds_e - ds}{ds} \tag{1}$$

The shape of the cable needs to satisfy the geometric constraint

$$(ds_e)^2 = (dx)^2 + (dy)^2 + (dz)^2 \tag{2}$$

Inserting Eq. (1) into Eq. (2) leads to $(1+\varepsilon)^2 = \|\partial \mathbf{r}/\partial s\|^2$. By omitting the second-order terms, we can get the axial strain as follows [15]:

$$\varepsilon = \frac{1}{2}\left(\frac{\partial \mathbf{r}^{\mathrm{T}}}{\partial s}\frac{\partial \mathbf{r}}{\partial s} - 1\right) = \frac{1}{2}\left[\left(\frac{\partial x}{\partial s}\right)^2 + \left(\frac{\partial y}{\partial s}\right)^2 + \left(\frac{\partial z}{\partial s}\right)^2 - 1\right] \tag{3}$$

Denote the position vector of P by $\mathbf{r}(s, t)$: $[t_0, \infty) \times [0, L] \to R^3$, where $\mathbf{r}(s, t) = [x(s,t), y(s,t), z(s,t)]^{\mathrm{T}}$ and t is the time variable. The unit vector $\mathbf{b}(s, t)$ tangent to the cable curve at point P can be obtained as

$$\mathbf{b}(s,t) = \frac{\partial s}{\partial s_e}\frac{\partial \mathbf{r}}{\partial s} = \frac{1}{1+\varepsilon}\frac{\partial \mathbf{r}}{\partial s} \tag{4}$$

The governing equation of a cable is given by

$$\rho \frac{d^2 \mathbf{r}(s,t)}{dt^2} = \frac{\partial}{\partial s}\left[EA\varepsilon(s,t)\mathbf{b}(s,t)\right] + \mathbf{a}(s,t) \tag{5}$$

where ρ is linear density of the unstretched cable, E is Young's modulus and A is the cross-sectional area of the cable. $\mathbf{a}(s, t)$ is the external force per unit length of the unstretched cable acting on it, and only the self-gravity of the cable is considered in this paper. So we have $\mathbf{a}(s, t) = \rho \mathbf{g}$, and $\mathbf{g}$ is the gravitational acceleration.

Inserting Eq. (4) into Eq. (5) leads to

$$\rho\frac{d^2\boldsymbol{r}(s,t)}{dt^2}=\frac{\partial}{\partial s}\left[\frac{EA\varepsilon(s,t)}{1+\varepsilon(s,t)}\right]\frac{\partial\boldsymbol{r}}{\partial s}+EA\frac{\varepsilon(s,t)}{1+\varepsilon(s,t)}\frac{\partial^2\boldsymbol{r}}{\partial s^2}+\boldsymbol{a}(s,t) \tag{6}$$

The velocity of point P with the curve length coordinate s can be obtained by differentiating $\boldsymbol{r}$ with respect to t in the following form:

$$\frac{d\boldsymbol{r}}{dt}=\frac{\partial\boldsymbol{r}}{\partial t}+\frac{\partial\boldsymbol{r}}{\partial s}\dot{s} \tag{7}$$

And the corresponding acceleration is

$$\frac{d^2\boldsymbol{r}}{dt^2}=\frac{\partial^2\boldsymbol{r}}{\partial t^2}+2\frac{\partial^2\boldsymbol{r}}{\partial s\partial t}\dot{s}+\frac{\partial^2\boldsymbol{r}}{\partial s^2}\dot{s}^2+\frac{\partial\boldsymbol{r}}{\partial s}\ddot{s} \tag{8}$$

where $\dot{s}=\mathrm{d}s/\mathrm{d}t$, $\ddot{s}=\mathrm{d}^2s/\mathrm{d}t^2$. For the cable-supporting system, cable lengths are changed slowly and smoothly, which leads to the assumption that $\dot{s}^2\approx 0$ and $\ddot{s}\approx 0$. Thus, Eq. (8) can be reduced to

$$\frac{d^2\boldsymbol{r}}{dt^2}=\frac{\partial^2\boldsymbol{r}}{\partial t^2}+2\frac{\partial^2\boldsymbol{r}}{\partial s\partial t}\dot{s} \tag{9}$$

The equation governing the cable dynamics can be obtained by inserting Eqs. (3), (4) and (9) into Eq. (6), which is a partial-differential equation with respect to the curve length coordinate s and time t.

3. Spatial discretization of cable dynamics equation

The finite-difference method is applied for the spatial discretization of Eq. (6). As shown in Fig. 3, the cable is equally distanced by $(n+1)$ nodes with $s_0=0$ and $s_n=L$. All the distances between two adjacent nodes are equal and of the form

$$l=L(t)/n \tag{10}$$

where $L(t)$ is the unstretched cable length at time t.

Using the central difference algorithm, the first order derivatives of the position vector of the ith ($i=1, 2, \ldots, n-1$) node can be expressed as

$$\frac{\partial\boldsymbol{r}_i}{\partial s}=\frac{\boldsymbol{r}_{i+1}-\boldsymbol{r}_{i-1}}{2l} \tag{11}$$

$$\frac{\partial^2\boldsymbol{r}_i}{\partial s^2}=\frac{\boldsymbol{r}_{i+1}-2\boldsymbol{r}_i+\boldsymbol{r}_{i-1}}{l^2} \tag{12}$$

Thus, the velocity and acceleration of the ith node can be obtained as

$$\frac{d\boldsymbol{r}_i}{dt}=\dot{\boldsymbol{r}}_i+\frac{\boldsymbol{r}_{i+1}-\boldsymbol{r}_{i-1}}{2l}\dot{s}_i \tag{13}$$

$$\frac{d^2\boldsymbol{r}_i}{dt^2}=\ddot{\boldsymbol{r}}_i+\frac{\dot{\boldsymbol{r}}_{i+1}-\dot{\boldsymbol{r}}_{i-1}}{l}\dot{s}_i+\frac{\boldsymbol{r}_{i+1}-\boldsymbol{r}_{i-1}}{l}\frac{\dot{l}}{l}\dot{s}_i \tag{14a}$$

where $\dot{s}_i=i\dot{l}/n$. By noting that in the third term on the right-hand side of Eq. (13), $\|(\boldsymbol{r}_{i+1}-\boldsymbol{r}_{i-1})/l\|\approx 2$, $\|\dot{l}/l\|\to 0$ and $\|\dot{s}\|\to 0$, Eq. (14a) can be further reduced to

$$\frac{d^2\boldsymbol{r}_i}{dt^2}=\ddot{\boldsymbol{r}}_i+\frac{\dot{\boldsymbol{r}}_{i+1}-\dot{\boldsymbol{r}}_{i-1}}{l}\dot{s}_i \tag{14b}$$

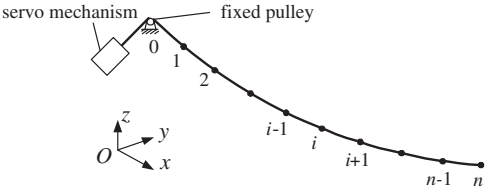

Fig. 3. Spatial discretization of a cable.

Substituting the velocity and acceleration of the nodes into Eq. (6) leads to

$$\rho\ddot{\boldsymbol{r}}_i+\rho\frac{\dot{\boldsymbol{r}}_{i+1}-\dot{\boldsymbol{r}}_{i-1}}{l}\dot{s}_i=EA\frac{1}{2l}\left(\frac{\varepsilon_{i+1}}{1+\varepsilon_{i+1}}-\frac{\varepsilon_{i-1}}{1+\varepsilon_{i-1}}\right)\frac{\boldsymbol{r}_{i+1}-\boldsymbol{r}_{i-1}}{2l}$$
$$+EA\frac{\varepsilon_i}{1+\varepsilon_i}\frac{\boldsymbol{r}_{i+1}-2\boldsymbol{r}_i+\boldsymbol{r}_{i-1}}{l^2}+\rho\boldsymbol{g}\quad(i=1,2,\ldots,n-1) \tag{15}$$

where $\varepsilon_i=1/2((\partial\boldsymbol{r}_i/\partial s)^{\mathrm{T}}(\partial\boldsymbol{r}_i/\partial s)-1)$.

Eq. (15) can be rewritten in the following form:

$$m_i\ddot{\boldsymbol{r}}_i+c_i\dot{\boldsymbol{r}}_{i-1}-c_i\dot{\boldsymbol{r}}_{i+1}+k_{i(i-1)}\boldsymbol{r}_{i-1}+k_{ii}\boldsymbol{r}_i+k_{i(i+1)}\boldsymbol{r}_{i+1}=\boldsymbol{f}_i,\quad i=1,2,\ldots,n-1 \tag{16}$$

where $m_i=\rho l$, $c_i=-\rho\dot{s}_i$,

$$k_{i(i-1)}=\frac{EA}{4l}\left(\frac{\varepsilon_{i+1}}{1+\varepsilon_{i+1}}-\frac{\varepsilon_{i-1}}{1+\varepsilon_{i-1}}\right)-\frac{EA}{l}\frac{\varepsilon_i}{1+\varepsilon_i},\quad k_{ii}=\frac{2EA}{l}\frac{\varepsilon_i}{1+\varepsilon_i},$$
$$k_{i(i+1)}=-\frac{EA}{4l}\left(\frac{\varepsilon_{i+1}}{1+\varepsilon_{i+1}}-\frac{\varepsilon_{i-1}}{1+\varepsilon_{i-1}}\right)-\frac{EA}{l}\frac{\varepsilon_i}{1+\varepsilon_i},\quad \boldsymbol{f}_i=\rho l\boldsymbol{g}.$$

Eq. (16) is the equation of motion of ith ($i=1, 2, \ldots, n-1$) node that applies to all the nodes of the cable, excepting the 0th and nth nodes on the cable ends. Accordingly, a set of nonlinear ordinary differential equations for the cable can now be obtained in the following form:

$$m_1\ddot{\boldsymbol{r}}_1+c_1\dot{\boldsymbol{r}}_0-c_1\dot{\boldsymbol{r}}_2+k_{10}\boldsymbol{r}_0+k_{11}\boldsymbol{r}_1+k_{12}\boldsymbol{r}_2=\boldsymbol{f}_1 \tag{17}$$

$$m_2\ddot{\boldsymbol{r}}_2+c_2\dot{\boldsymbol{r}}_1-c_2\dot{\boldsymbol{r}}_3+k_{21}\boldsymbol{r}_1+k_{22}\boldsymbol{r}_2+k_{23}\boldsymbol{r}_3=\boldsymbol{f}_2 \tag{18}$$

$$m_3\ddot{\boldsymbol{r}}_3+c_3\dot{\boldsymbol{r}}_2-c_3\dot{\boldsymbol{r}}_4+k_{32}\boldsymbol{r}_2+k_{33}\boldsymbol{r}_3+k_{34}\boldsymbol{r}_4=\boldsymbol{f}_3 \tag{19}$$

$$\vdots$$

$$m_{n-2}\ddot{\boldsymbol{r}}_{n-2}+c_{n-2}\dot{\boldsymbol{r}}_{n-3}-c_{n-2}\dot{\boldsymbol{r}}_{n-1}+k_{(n-2)(n-3)}\boldsymbol{r}_{n-3}+k_{(n-2)(n-2)}\boldsymbol{r}_{n-2}$$
$$+k_{(n-2)(n-1)}\boldsymbol{r}_{n-1}=\boldsymbol{f}_{n-2} \tag{20}$$

$$m_{n-1}\ddot{\boldsymbol{r}}_{n-1}+c_{n-1}\dot{\boldsymbol{r}}_{n-2}-c_{n-1}\dot{\boldsymbol{r}}_n+k_{(n-1)(n-2)}\boldsymbol{r}_{n-2}+k_{(n-1)(n-1)}\boldsymbol{r}_{n-1}$$
$$+k_{(n-1)n}\boldsymbol{r}_n=\boldsymbol{f}_{n-1} \tag{21}$$

We can note from Eq. (16) or the above equations that the equation of motion of each node involves the position and velocity of its adjacent nodes; consequently, Eq. (16) cannot be directly employed to describe the motion of the nodes located at the cable ends, namely, node 0 and n. Since Eqs. (17) and (21) involve the 0th and nth nodes, respectively, we rewrite Eqs. (17) and (21) as follows:

$$m_1\ddot{\boldsymbol{r}}_1-c_1\dot{\boldsymbol{r}}_2+k_{11}\boldsymbol{r}_1+k_{12}\boldsymbol{r}_2=\tilde{\boldsymbol{f}}_1 \tag{22}$$

$$m_{n-1}\ddot{\boldsymbol{r}}_{n-1}+c_{n-1}\dot{\boldsymbol{r}}_{n-2}+k_{(n-1)(n-2)}\boldsymbol{r}_{n-2}+k_{(n-1)(n-1)}\boldsymbol{r}_{n-1}=\tilde{\boldsymbol{f}}_{n-1} \tag{23}$$

in which, $\tilde{\boldsymbol{f}}_1=\boldsymbol{f}_1-c_1\dot{\boldsymbol{r}}_0-k_{10}\boldsymbol{r}_0$, $\tilde{\boldsymbol{f}}_{n-1}=\boldsymbol{f}_{n-1}+c_{n-1}\dot{\boldsymbol{r}}_n-k_{(n-1)n}\boldsymbol{r}_n$.

By defining

$$\boldsymbol{x}=[\boldsymbol{r}_1^T\ \boldsymbol{r}_2^T\ \cdots\ \boldsymbol{r}_{n-1}^T]^T,\quad \boldsymbol{m}=diag(m_1\boldsymbol{I},m_2\boldsymbol{I},\cdots,m_{n-1}\boldsymbol{I}),$$

$$\boldsymbol{c}=\begin{bmatrix}0 & -c_1\boldsymbol{I} & 0 & 0 & \cdots & 0 & 0 & 0\\ c_2\boldsymbol{I} & 0 & -c_2\boldsymbol{I} & 0 & \cdots & 0 & 0 & 0\\ 0 & c_3\boldsymbol{I} & 0 & -c_3\boldsymbol{I} & \cdots & 0 & 0 & 0\\ \cdots & \cdots & \cdots & \cdots & \cdots & \cdots & \cdots & \cdots\\ 0 & 0 & 0 & 0 & \cdots & c_{n-2}\boldsymbol{I} & 0 & -c_{n-2}\boldsymbol{I}\\ 0 & 0 & 0 & 0 & \cdots & 0 & c_{n-1}\boldsymbol{I} & 0\end{bmatrix}$$

$$\boldsymbol{k}=\begin{bmatrix} k_{11}\boldsymbol{I} & k_{12}\boldsymbol{I} & 0 & 0 & \cdots & 0 & 0 & 0 \\ k_{21}\boldsymbol{I} & k_{22}\boldsymbol{I} & k_{23}\boldsymbol{I} & 0 & \cdots & 0 & 0 & 0 \\ 0 & k_{32}\boldsymbol{I} & k_{33}\boldsymbol{I} & k_{34}\boldsymbol{I} & \cdots & 0 & 0 & 0 \\ \cdots & \cdots & \cdots & \cdots & \cdots & \cdots & \cdots & \cdots \\ 0 & 0 & 0 & 0 & \cdots & k_{(n-2)(n-3)}\boldsymbol{I} & k_{(n-2)(n-2)}\boldsymbol{I} & k_{(n-2)(n-1)}\boldsymbol{I} \\ 0 & 0 & 0 & 0 & \cdots & 0 & k_{(n-1)(n-2)}\boldsymbol{I} & k_{(n-1)(n-1)}\boldsymbol{I} \end{bmatrix}$$

$$\boldsymbol{f}=\begin{bmatrix}\tilde{\boldsymbol{f}}_1^T & \boldsymbol{f}_2^T & f_3^T & \cdots & \boldsymbol{f}_{n-2}^T & \tilde{\boldsymbol{f}}_{n-1}^T\end{bmatrix}^T$$

where $\boldsymbol{I}$ is the 3×3 identity matrix, Eqs. (22), (18)–(20) and (23) can be rewritten as

$$\boldsymbol{m}\ddot{\boldsymbol{x}}+\boldsymbol{c}\dot{\boldsymbol{x}}+\boldsymbol{k}\boldsymbol{x}=\boldsymbol{f} \tag{24}$$

Eq. (24) is a nonlinear second-order ordinary differential equation of $3(n-1)$ variables. It needs to be pointed out that (1) $\boldsymbol{x}$ is the absolute nodal coordinates of the cable nodes instead of their displacement; (2) $\boldsymbol{c}$ is the matrix resulted from the rate of the change in the cable length, which acts as a damping matrix. Structural damping is not taken into account in the paper; (3) $\boldsymbol{k}$ is the stiffness matrix depending on the strain of the cable; (4) the matrices $\boldsymbol{m}$, $\boldsymbol{k}$ and $\boldsymbol{f}$ depend on the cable length at the current moment, and $\boldsymbol{c}$ on the rate of the change in the cable length. The advantage of dividing a cable into a constant number of nodes is that the number of DOF of a cable keeps constant, which significantly decreases the difficulty in the control problem of cable vibration suppression compared with the model of a varying number of nodes. We also note that subscript j for the jth cable is omitted in the former equations that are applied to all the cables of the manipulator.

Boundary conditions and the initial states of the cable need to be introduced to solve Eq. (24), which will be given in the next section.

4. Dynamics model of CDPMs

The end-effector has a local coordinate frame E_1 fixed on it with the origin located at its centroid. The position of the local coordinate frame is given by $\boldsymbol{h}=[x\ y\ z]^{\mathrm{T}}$, and the orientation is given by $\boldsymbol{\psi}=[\alpha\ \beta\ \gamma]^{\mathrm{T}}$. We choose the orientation to be given by the X–Y–Z Euler angles. Thus the pose of the end-effector can be described by

$$\boldsymbol{q}=[\boldsymbol{h}^{\mathrm{T}}\boldsymbol{\psi}^{\mathrm{T}}]^{\mathrm{T}}=[x\quad y\quad z\quad \alpha\quad \beta\quad \gamma]^{\mathrm{T}} \tag{25}$$

The resultant force, $\boldsymbol{f}_r$, and moment, $\boldsymbol{m}_r$, on the end-effector exerted by the cables can be obtained by summing all the cable end forces in the following form:

$$\boldsymbol{f}_r=-\sum_{j=1}^{nc}\boldsymbol{p}_j \tag{26}$$

$$\boldsymbol{m}_r=-\sum_{j=1}^{nc}\boldsymbol{s}_j\times\boldsymbol{p}_j \tag{27}$$

where $\boldsymbol{p}_j$ ($j=1, 2, \ldots, nc$) stands for the cable tension at its end connecting to the end-effector, namely, that at the nth node. nc is the number of cables that move the end-effector. Since $\boldsymbol{p}_j$ is the cable tension at its last node, the central difference algorithm does not work; however, $\boldsymbol{p}_j$ can be straightly obtained by dealing with the cable segment between its $(n-1)$th and nth nodes as a linear element that can only work in tension.

The equation of motion of the manipulator can be written in the following general form:

$$\boldsymbol{M}(\boldsymbol{q})\ddot{\boldsymbol{q}}+\boldsymbol{C}(\boldsymbol{q},\dot{\boldsymbol{q}})+\boldsymbol{G}(\boldsymbol{q})=\boldsymbol{\tau} \tag{28}$$

where $\boldsymbol{M}(\boldsymbol{q})$ is the inertia matrix of the manipulator, $\boldsymbol{C}(\boldsymbol{q},\dot{\boldsymbol{q}})$ is the Coriolis and centripetal term, $\boldsymbol{G}(\boldsymbol{q})$ is the vector of gravity term. $\boldsymbol{\tau}=[\boldsymbol{f}_r^T\ \boldsymbol{m}_r^T]^T$ is the wrench exerted on the end-effector by cables.

The position vector of the attachment point of the jth cable on the end-effector is denoted by $\boldsymbol{d}_j$, ($j=1, 2,\ldots, nc$), in the local coordinate frame E_1. It may be expressed in the global coordinate frame as

$$\boldsymbol{x}_{jn}=\boldsymbol{h}+\boldsymbol{T}\boldsymbol{d}_j,\quad (j=1,2,\ldots,nc) \tag{29}$$

where $\boldsymbol{T}$ is the rotation matrix of the local coordinate frame E_1 with respect to the global coordinate frame, which can be written as

$$\boldsymbol{T}=\begin{bmatrix} c\beta c\gamma & -c\beta s\gamma & s\beta \\ s\alpha s\beta c\gamma+c\alpha s\gamma & -s\alpha s\beta s\gamma+c\alpha c\gamma & -s\alpha c\beta \\ -c\alpha s\beta c\gamma+s\alpha s\gamma & c\alpha s\beta s\gamma+s\alpha c\gamma & c\alpha c\beta \end{bmatrix} \tag{30}$$

in which $c(\cdot)$ and $s(\cdot)$ stand for the cosine and sine of the argument, respectively.

The velocity of the attachment point of the jth cable can be obtained by differentiating Eq. (29) with respect to time t as

$$\dot{\boldsymbol{x}}_{jn}=\dot{\boldsymbol{h}}+[\boldsymbol{\omega}\times]\boldsymbol{d}_j,\quad (j=1,2,\ldots,nc) \tag{31}$$

where $[\boldsymbol{\omega}\times]=\dot{\boldsymbol{T}}\boldsymbol{T}^{\mathrm{T}}$ and $\boldsymbol{\omega}$ is the angular velocity of the end-effector, which depends on $\boldsymbol{\psi}$ and $\dot{\boldsymbol{\psi}}$.

Eqs. (29) and (31) are the boundary conditions for the nth node of the jth cable. And for the 0th node of the jth cable we have

$$\boldsymbol{x}_{j0}=\boldsymbol{P}_j,\quad \dot{\boldsymbol{x}}_{j0}=0,\quad (j=1,2,\ldots,nc) \tag{32}$$

where $\boldsymbol{P}_j$ is the position vector of the attachment point of the jth cable connecting to the base.

In the initial state $t=0$, the manipulator is supposed to be in the static equilibrium state that can be obtained using the method presented in Ref. [7]. Thus, combining Eqs. (24) and (28) yields to the motion of equation of the CDPM, which can be solved numerically using the common fourth-order Runge–Kutta method.

5. Numerical examples

This section provides two numerical examples to validate the dynamics model of the CDPM involving time-varying cable length. First, a planar CDPM with two cables is simulated, and a comparison is made to a mass-spring model created using ADAMS software, a multibody dynamics package. Then, the cable-supporting system is analyzed to investigate the effects of cable vibrations on the positioning precision of the end-effector.

5.1. Planar CDPM with 2 cables

The planar CDPM is shown in Fig. 4 where cable AB and cable BC are connected to the point mass m at B. The other end A of cable AB is fixed on the base, and the other end of cable BC is fed through a fixed pulley, and then is pulled vertically downwards at point D. The tangent point where cable BC touches the pulley is denoted by C. The curve length between BC can be changed by exerting a motion or a force on the point D vertically so that the point mass m will be moved in the vertical plan defined by Oxy.

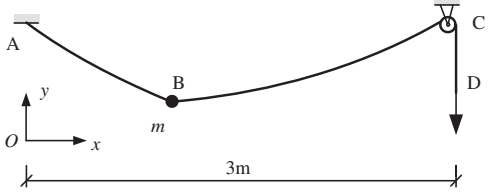

Fig. 4. Planar 2-cable-driven parallel manipulator.

The parameters of the planar manipulator are listed in Table 1. In this example, we designate a relative large value to ρ while relative small values to EA and m in order that the effect of cable vibration on the mass can be easily observed. In the initial state, the manipulator is in the static equilibrium state, and curve of cable AB and BC can be described using catenary equation. The acceleration of gravity $\boldsymbol{g}=[0,\ -9.8]^{\mathrm{T}}$.

It needs to be pointed out that tangent point C is the point where cable BC meets the pulley in the initial state, however, in the simulation of the manipulator using the methodology presented in the paper, this point is supposed to be fixed, namely, not changed while the curve length of cable BC changes. In this example, cables AB and BC are divided into 8 and 11 nodes, respectively.

To make a comparison with the simulated results, a mass-spring model shown in Fig. 5 is created using the ADAMS software to simulate the dynamical behaviors of the manipulator. The cables are treated as a series of small spherical bodies, representing the masses concentrated on the nodes, connected with springs, and a contact pair is created between each node and the pulley. The nodes of the cables slide smoothly through the pulley when a motion is exerted on the point D vertically. The radius of the pulley is assumed to be 0.08 m.

The motion exerted on point D is described as $\Delta L(t)=0.15\sin(0.8\pi t)$ and the simulation duration is 5 s. The motion of the point mass m in the x and y directions is plotted in Fig. 6 where the solid line is the result obtained with the proposed method and the dot line is that with the mass-spring model, and the difference between the two methods is given in Fig. 7. The maximal displacements in the x and y directions are 0.10 m and 0.25 m, respectively; and the differences in the x and y directions are 0.005 m and 0.015 m, respectively. The relative differences ($\|\Delta\boldsymbol{r}_1-\Delta\boldsymbol{r}_2\|/\|\Delta\boldsymbol{r}_2\|\times 100\%$) between the two methods are within 8.0% in both x and y directions, which can also be roughly estimated as ($\max(\|\Delta\boldsymbol{r}_1-\Delta\boldsymbol{r}_2\|)/\max(\|\Delta\boldsymbol{r}_2\|)\times 100\%$), where $\Delta\boldsymbol{r}_1$ and $\Delta\boldsymbol{r}_2$ are the displacements of the point mass m with respect to its initial state obtained with the proposed method and the mass-spring model, respectively.

The good match between the results shows that the methodology presented in the paper is efficient to simulate the dynamical behaviors of cables with time-varying length. The difference between the results mainly comes from the fact that the tangent point C varies with the changing cable length. Fig. 8 presents the dynamic profiles of the cables at different instants from $t=0$ to 1.9 s. It is seen that the nonlinear behavior of the cable vibration is very complicated. The proposed method can detect the dynamic behavior of varying-length cables effectively, and it can be directly employed to investigate the effects of cable vibration on the positioning precision of the end-effector.

Table 1
Parameter values of the planar manipulator.

System parameters	Value
Position of point A	(−1.0, 1.0) m
Position of point C	(2.0, 1.0) m
Position of point B in initial state	(0.00177, 0.50529) m
Axial stiffness of cables EA	6.5973×10^4 N
Mass per unit length of cables ρ	0.204 kg/m

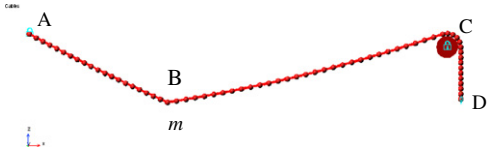

Fig. 5. Mass-spring model of the planar manipulator.

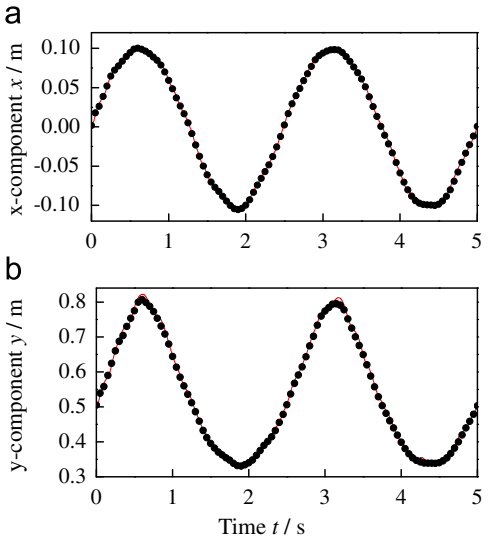

Fig. 6. Motion of the point mass m.

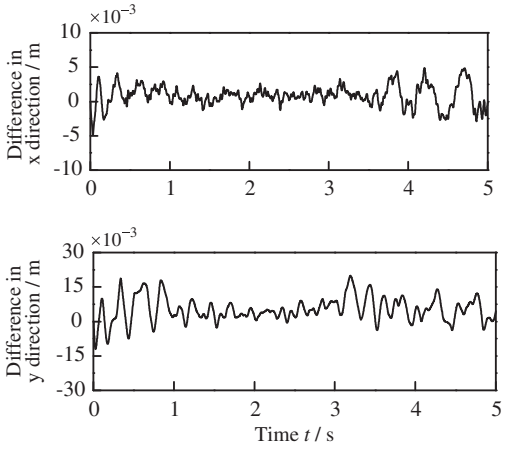

Fig. 7. Difference between results of the two models.

It should be pointed out that in the mass-spring model created in ADAMS software the distance between two adjacent nodes needs to be less than the radius of the fixed pulley in order to enable smooth contacts between the cable and the pulley. Therefore, the cable BC is divided into 30 mass-spring elements. The fact that the radius of the pulley is several orders less than the cable length in engineering results in too many mass-spring elements. Furthermore, the integration step size for solving the mass-spring model should be small enough to detect and simulate the dynamic contact behavior between the nodes and the pulley. Therefore, the model created in ADAMS is much more time-consuming than the proposed method because of the large amount of mass-spring elements divided for the cable and the existence of a great number of contact pairs. And too many contact pairs also lead to relatively more failures in numerical integration.

5.2. Cable-supporting system of the FAST scaled model

In the scaled model of the FAST cable-supporting system as shown in Fig. 2, a hemisphere shell with the radius of 0.50 m serves as the end-effector. The parameters of the manipulator are given in

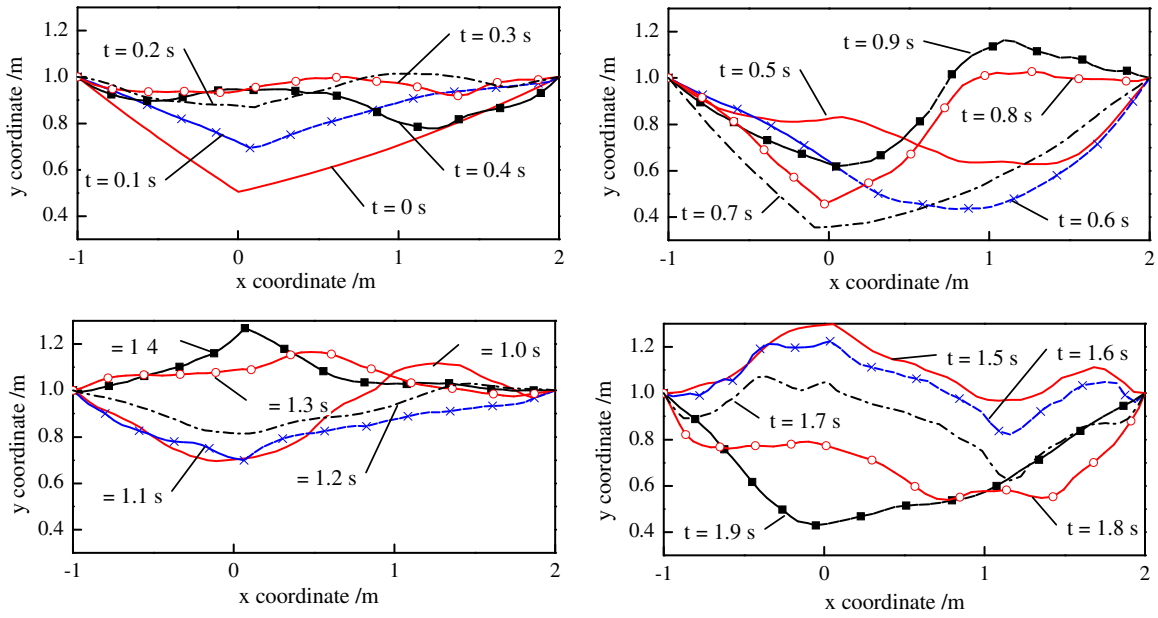

Fig. 8. Dynamic profiles at different instants t=0–1.9 s.

Table 2
Parameters of FAST50m cable-driven manipulator.

System parameters	Value
Axial stiffness of the cable EA	2.39×10^6 N
Weight per unit length of the cable ρ	0.14 kg/m
Poisson's ratio of the cable	0.3
Mass of the end-effector	120 kg
Moment of inertia of the end-effector	diag(33.97, 33.97, 54.34) kg m^2

Table 3
Position of pulleys and cable attachment points.

No	Pulley position in the global frame (m)	Cable attachment point position in local frame (m)
1	(−24.853, 0.016, 20.987)	(0.091, 0.517, −0.140)
2	(−12.474, −21.492, 21.012)	(−0.175, 0.109, 0.406)
3	(12.375, −21.519, 20.984)	(−0.493, −0.179, −0.140)
4	(24.777, 0.006, 20.986)	(−0.007, −0.206, 0.406)
5	(12.368, 21.490, 20.990)	(0.402, −0.337, −0.140)
6	(−12.449, 21.500, 20.986)	(0.182, 0.097, 0.406)

Table 2 and the position of the 6 fixed pulleys in the global coordinate frame and that of the 6 cable attachment points in the local coordinate frame attached to the end-effector are listed in Table 3. Each cable is divided into 21 equal-distanced nodes.

The initial pose of the end-effector is given as $\boldsymbol{q}_1$=(1.00, 1.00, 15.00, 0.0816, −0.0813, 3.108)$^{\mathrm{T}}$ and the terminal pose is supposed to be $\boldsymbol{q}_2$=(2.00, 2.00, 16.00, 0.176, −0.174, 3.120)$^{\mathrm{T}}$. Here, and in the subsequent examples, the SI units (m, kg, s, rad) are used for all quantities. The manipulator is asked to accomplish the line from $\boldsymbol{q}_1$ to $\boldsymbol{q}_2$ in T_1=10 s, and then rests at $\boldsymbol{q}_2$. The trajectory can be described as $\boldsymbol{q}(t)=\boldsymbol{q}_1+\boldsymbol{v}t$, where $\boldsymbol{v}=(\boldsymbol{q}_2-\boldsymbol{q}_1)/T_1$, and we can see $\|\boldsymbol{v}\|$=0.1732 m/s. The simulation duration is supposed as T=14 s. Due to the slow motion of the manipulator during observing radio targets in the space, the manipulator can be considered in the static state at an arbitrary instant during the motion. Therefore, a static model can be utilized to describe the dynamic behavior of the manipulator. During the line motion, the change in the cable length is obtained using the static model as presented in Ref. [7]. The vibration of the end-effector obtained according to the proposed method with respective to the static configuration is shown in Fig. 9.

We can note from Fig. 9 that the vibration of the end-effector occurs around its corresponding static pose during the motion of the manipulator. The amplitude of the translational vibration ($(\Delta x^2+\Delta y^2+\Delta z^2)^{1/2}$) is approximately 7.5 mm, and that of the rotational vibration is 8.25×10^{-3} rad (0.47°). From these results we can see that the deviation between the result based on the dynamic model and that based on the static model is relatively trivial. The maximal translational velocity of the FAST 50 m model during observing operation is demanded to be 2 cm/s, which is much less than that used in the simulation. Therefore, it can be concluded that the dynamic behavior of the cable-supporting system is so trivial that it can be neglected due to its slow motion during observing operation. Thus, the assumption in Refs. [7,16] that the cable-supporting system can be treated as in the static state is reasonable.

We find, however, that this assumption holds true only if there is no pose error of the end-effector at the initial instant and the length of the cables changes slowly and smoothly. If otherwise, the vibration of the manipulator can be observed obviously and it attenuates very slowly due to the low damp of cables. An example of a line motion from $\boldsymbol{q}_1$ to $\boldsymbol{q}_3$ is presented to demonstrate the vibration resulted from the initial pose error. The initial pose of the end-effector is measured to be $\boldsymbol{q}_1$=(1.00, 1.00, 15.00, 0.0816, −0.0813, 3.108)$^{\mathrm{T}}$ using measuring devices with random measurement errors. And the real pose of the end-effector is $\boldsymbol{q}_{10}$=(1.02, 1.02, 15.02, 0.0816, −0.0813, 3.108)$^{\mathrm{T}}$. The manipulator is asked to move in 10 s to the terminal pose $\boldsymbol{q}_3$=(2.50, 1.50, 16.2, 0.135, −0.263, 3.121)$^{\mathrm{T}}$. In the case that the measured pose $\boldsymbol{q}_1$ is utilized as the starting pose to calculate the change in the cable length for the line motion, the motions of the manipulator based on the proposed dynamic model and that based on the static model are plotted in Fig. 10. Here for the space limitation only the x and α components of the motion are given, and the other components are of the similar

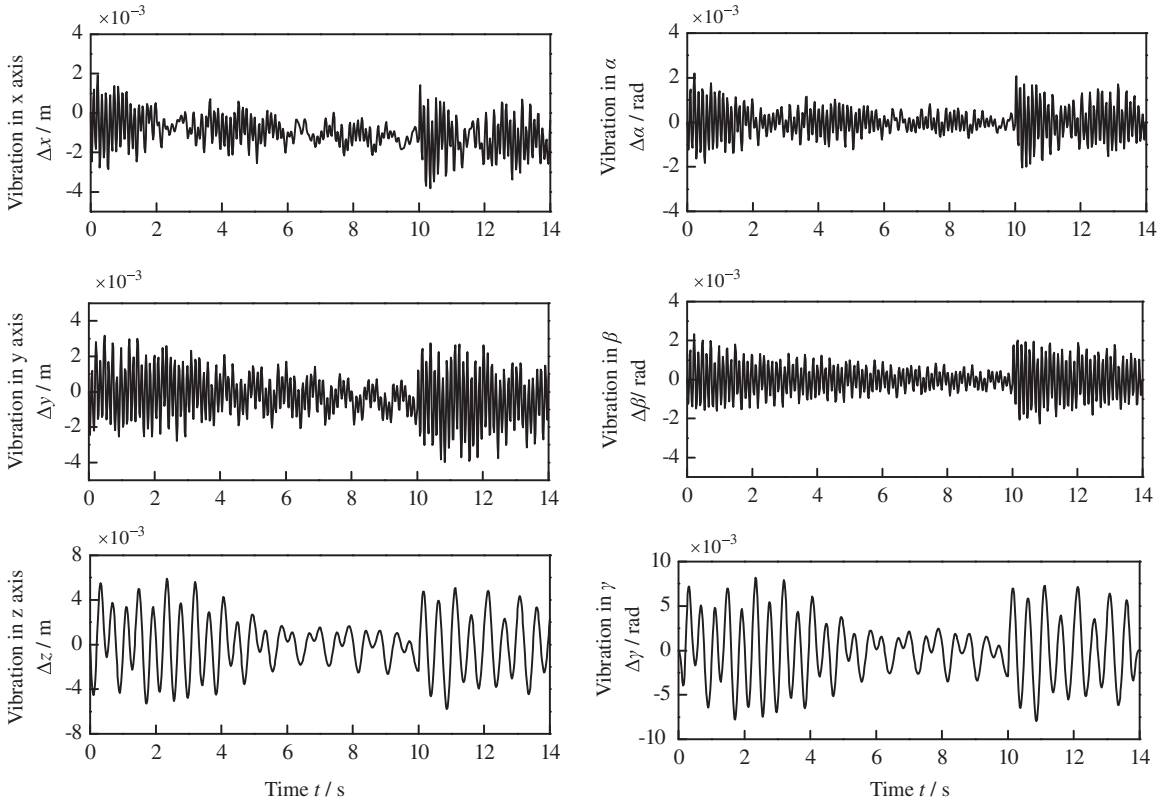

Fig. 9. Vibration of the end-effector with respect to its static configuration.

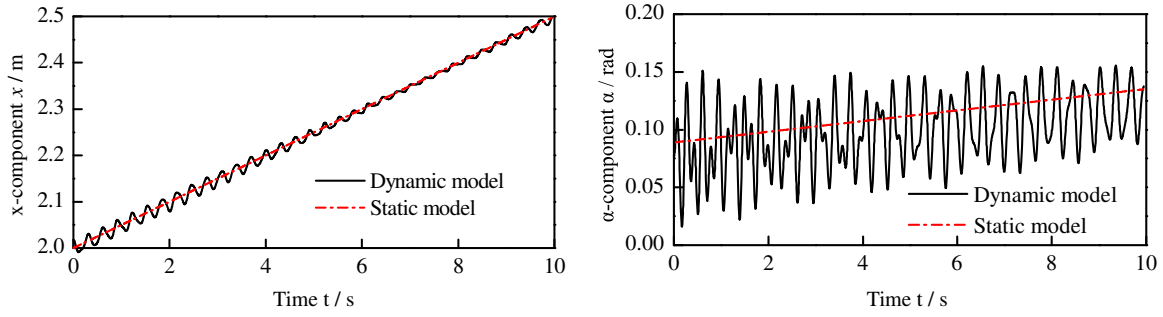

Fig. 10. Comparison between dynamic and static motions with initial error.

form. The vibration of the end-effector around its static pose is shown in Fig. 11.We can see that the vibration of the manipulator exists during the motion and it attenuates very slowly. The amplitude of the translational vibration is approximately 35 mm, and that of the rotational vibration is 80×10^{-3} rad (4.6°).

It is observed that the vibration of the manipulator will increase with an increasing operation velocity, leading to a larger vibration from its static pose of the manipulator. Therefore, the dynamic behavior of the manipulator must be taken into consideration in the case that the manipulator operates with a large velocity, or in order to eliminate the vibration of the cables effectively.

6. Conclusions

This paper addresses the modeling of large CDPMs, for which the dynamic behavior of the cables must be taken into consideration. The dynamic model proposed for large CDPMs can be readily utilized to estimate the effects of the cable vibrations on the positioning precision of the end-effector, and further to eliminate the vibrations of the manipulator, guaranteeing smooth motion of the manipulator with high positioning precision.

It is noted that the items involving $\dot{s}$ can be also be omitted in Eq. (24) when the cable length changes very slowly. Thus, the dynamics of the manipulator reduces to a structural vibration problem with a moving equilibrium position. Generally, only the first two or three vibration modes are needed to be taken in account in engineering; therefore, cables can only be divided into several nodes to include these modes, leading to an acceptable model in the viewpoint of time consumption.

Determining whether the items involving $\dot{s}$ and/or $\ddot{s}$ can be neglected according to the rate of change in cable length, and the appropriate number of nodes for a cable to be divided is still a key problem to be further investigated.

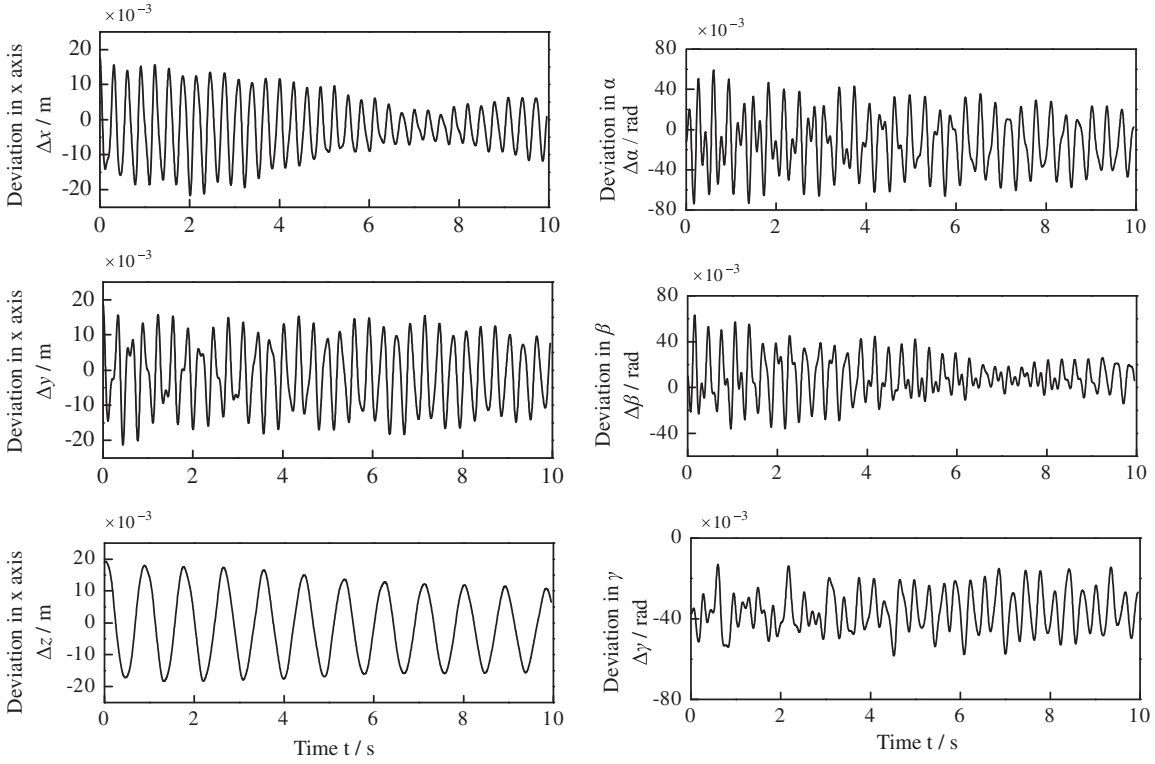

Fig. 11. Vibration of the end-effector with initial error.

Acknowledgments

The authors would like to thank the National Natural Sciences Foundation of China under Grants 51105290 and 51175397, and the Fundamental Research Funds for the Central Universities under Grants JY10000904011, JY10000904006, JY10000904013 and JY10000904019. The authors also deeply appreciate the numerous remarks and suggestions of anonymous referees, which led to improvements in this paper.

References

[1] B.Y. Duan, Y.Y. Qiu, F.S. Zhang, et al., On design and experiment of the feed cable-suspended structure for super antenna, Mechatronics 19 (4) (2009) 503–509.
[2] Y.X. Su, B.Y. Duan., The application of the Stewart platform in large spherical radio telescopes, J. Robotic Syst. 17 (7) (2000) 375–383.
[3] B.Y. Duan, J.L. Du, On analysis and optimization of an active cable-mesh main reflector for a giant Arecibo-type antenna structural system, IEEE Trans. Antennas Propag. 55 (5) (2007) 1222–1229.
[4] M. Gouttefarde, C. Gosselin, Analysis of the wrench-closure workspace of planar parallel cable-driven mechanisms, IEEE Trans. Robotics 22 (3) (2006) 434–445.
[5] H.D. Taghirad, M.A. Nahon, Dynamic analysis of a macro-micro redundantly actuated parallel manipulator, Adv. Robotics 22 (9) (2008) 949–981.
[6] S.R. Oh, S.K. Agrawal., A reference governor based controller for a cable robot under input constraints, IEEE Trans. Control Syst. Technol. 13 (4) (2005) 639–645.
[7] Y.Y. Qiu, B.Y. Duan, Q. Wei, et al., Elimination of force singularity of the cable and cabin structure for the next generation large radio telescope, Mechatronics 12 (7) (2002) 905–918.
[8] Jingli Du, Hong Bao, Xuechao Duan, Chuanzhen Cui, Jacobian analysis of a long-span cable-driven manipulator and its application to forward solution, Mech. Mach. Theory 45 (9) (2010) 1227–1238.
[9] C.G. Koh, Y. Rong, Dynamic analysis of large displacement cable motion with experimental verification, J. Sound Vib. 272 (1-2) (2004) 187–206.
[10] L.Q. Chen, H. Ding., Two nonlinear models of a transversely vibrating string, Arch. Appl. Mech. 78 (5) (2008) 321–328.
[11] V. Gattulli, R. Alaggio, F. Potenza, Analytical prediction and experimental validation for longitudinal control of cable oscillations, Int. J. Non-Linear Mech. 43 (1) (2008) 36–52.
[12] Y. Terumichi, M. Ohtsuka, M. Yoshizawa, et al., Nonstationary vibrations of a string with time-varying length and a mass-spring system attached at the lower end, Nonlinear Dyn. 12 (1) (1997) 39–55.
[13] P.H. Wang, R.F. Fung, M.J. Lee, Finite element analysis of a three-dimensional underwater cable with time-dependent length, J. Sound ib. 209 (2) (1998) 223–249.
[14] Q.J. Duan, J.L. Du, B.Y. Duan, A.F. Tang, Deployment/retrieval modeling of cable-driven parallel robot, Math. Probl. Eng. 2010 (2010) 1–10.
[15] Y.Q. Ni, W.J. Lou, J.M. Ko, A hybrid pseudo-force/laplace ransform method for non-linear transient response of a suspended cable, J. Sound Vib. 238 (2) (2000) 189–214.
[16] K. Kozak, Q. Zhou, J. Wang, Static analysis of cable-driven manipulators with non-negligible cable mass, IEEE Trans. Robotics 22 (3) (2006) 425–433.